# LOW VOLTAGE ELECTRON BEAM BUNCHING AND DEFLECTION*

M. Cavenago§, INFN/LNL, Legnaro (PD) Italy

F. Cavaliere, G. Maero, B. Paroli, R. Pozzoli, M. Romé,

Università degli Studi di Milano e INFN, Milano, Italy

## Abstract

The propagation and deflection of a 1 to 10 keV electron beam through a a Malmberg-Penning trap is described, with the development of a vectorized and symplectic partitioned transport code. The experimental setup includes a laser which is back-scattered by pulsed electron bunches, produced by an external photocathode source with 4 ns length, so that Thomson scattering diagnostics can be tested and compared to other installed diagnostics. Both the laser and the electron dump are described.

## INTRODUCTION AND SETUP

The Malmberg-Penning trap ELTRAP[1] was originally designed to store electrons accelerated by low voltages (100 V) in a highly uniform magnetic field, to produce a non-neutral plasma. In the recent ELTEST experiment, the collision between 4ns electron bunches produced by an external source in the 2 to 10 keV energy range and a laser beam beam (L2 in fig 1) is studied, as a test of the Thomson scattering diagnostic. Six photomultiplier (PMT) windows are placed around the CF35 laser input pipe. In order to measure the very few Thomson backscattered photons, proper dumping of the laser and of the electron beams are required. The longitudinal expansion of the electron bunch due to space charge can be measured by an electrostatic diagnostics[2]; proper software is needed to compensate for the capacitance of the pickup electrodes.

A schematic view of the experimental apparatus is shown in fig 1, where $z$ is the main solenoid axis and $z = 0$ its middle plane; external beam source is at $z = -1.41$ m, while main laser input viewport is at $z = 1.36$ m; eight lateral CF63 flanges for $e^-$ dumps are placed at $r = 0.125$ m, centered about $z_c = 1.1$ m, and may be equipped with removable phosphor screens to detect the deflected beam. The off-axis deflection of the electrons is complicated by the magnetic field but was recently demonstrated. Its optimization needs development of a vectorized code for crossed electric and magnetic fields.

Laser L2 collimated to a 6 mm diameter makes a 10.6 mrad angle with the $z$ axis, crossing it at $z = 0.33$ m, so that L2 travels 17 mm under the $z$ axis at $z = -1.3$ m, where the laser dump is located. The dump consists of a mirror, deviating L2 outside of the vacuum chamber through a bottom CF63 port onto an absorber. The mirror is protected from electrons by a 16 mm diameter 60 mm long drift tube, sustained through a pole by the same CF63 flange. The pole is
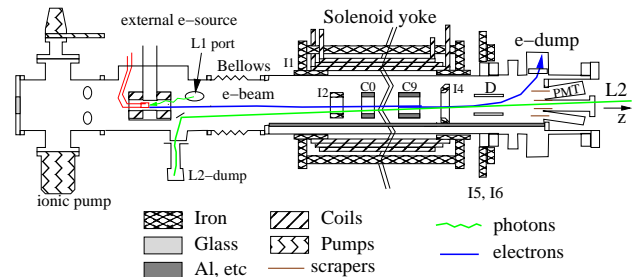
Figure 1: Experimental set-up: L1= UV laser extracting electrons; L2 = main laser; PMT = photomultipliers; D = deflector; $C_i$ electrodes; $I_i$ iron shims

designed to minimize rf dipole effects, similar to the Quarter Wave Resonator case[3].

A bunched electron beam[4] is generated by a photocathode source heated at 1050 K and illuminated by a $t_d = 4$ ns pulse from an UV laser L1 ($\lambda = 337$ nm). A local magnetic field $\mathbf{B}^H$ (generated by a Helmholtz-coil pair with a 1% uniformity over a distance of 13mm from the emitter) provides the initial focusing of the emitted electrons. This field is much less, $|\mathbf{B}_z^H| < 50$ G, than the main solenoid field $B_z < 2$ kG, but can be easily reversed. The source is held at a fixed potential $V_s$ (adjustable from -1.1 kV to -10 kV) with respect to the grounded vacuum chamber, and electron bunches with total charge from 0.5 pC to 50 pC can be obtained. From the Child-Langmuir limit on extracted current, $|V_s| > 1.3 \pm 0.2$ kV in our source geometry.

## ELECTRON BEAM SIMULATIONS

Electron beam deflection and scrapers have the purpose of avoiding direct illumination of the PMT window from the electron beam. The deflector is partly shielded from the main solenoid field, since this exerts a strong guiding effect of the electron beam. Let $\mathbf{E}$ be the applied electric field, $\mathbf{B}$ the applied magnetic field and $\mathbf{E}_s$ the field generated by the beam space charge. For reasonable large source voltage $|V_s| < 5$ kV, the self field $\mathbf{E}_s$ is small compared to $\mathbf{E}$ (except for the acceleration gap in the electron source, excluded from these global simulations) and will be here neglected.

Without deflection field, the electron beam radius $r_b$ will expand as $r_b \cong r_0 \sqrt{B_0/B_z(0,0,z)}$. In the deflector we have $B_z^d = 0.03$ T when $B_0 = 0.1$ T, and $E^d \cong 1$ kV/cm; in the well known drift approximation, electrons will tend to acquire a transverse velocity $\mathbf{v}_d = \mathbf{E}^d \times \mathbf{B}^d / |\mathbf{B}^d|^2$ while they maintain their longitudinal velocity $v_z \cong c\beta$, with $\beta \cong 0.18$ for a typical source voltage $V_s = -8$ kV. After the deflector $\mathbf{v}_d$ vanishes again, but the beam has moved off-axis, so

**03 Linear Colliders, Lepton Accelerators and New Acceleration Techniques**

**D04 High Intensity in Linear Accelerators - Incoherent Instabilities, Space Char**
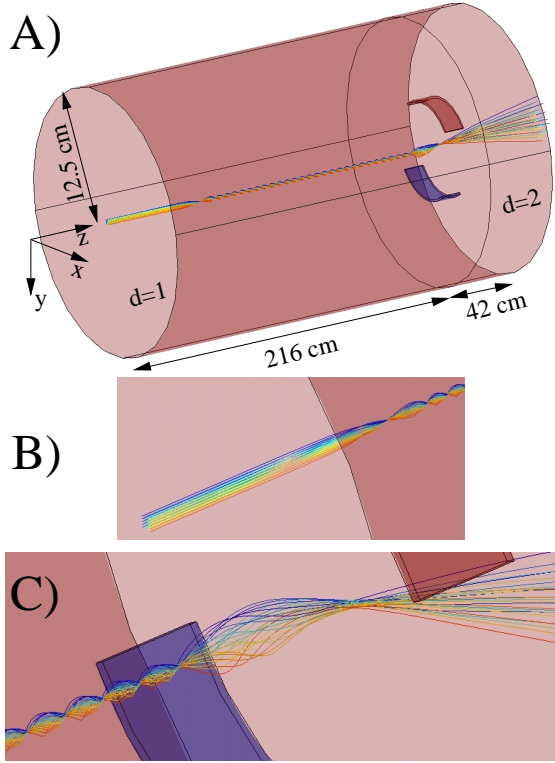
Figure 2: A) Domains $d = 1$ and 2 of simulation geometry; deflector negative electrode marked in blue; B) zoom on beam compression region; C) zoom on beam deflection

that the diverging magnetic field now completes the electron deflection. The need to integrate several simulations together leaded us to developed some particle tracing tools in the Comsol Multiphysics 3.5 (TM) environment[5]; the status of these tools is here described.

A view of the beam simulation region is in fig 2A. The magnetic field is computed in cylindrical coordinates $r, z$; simulation region is a large sphere $\sqrt{r^2 + z^2} \leq 2$ m, and at its boundary, the field is matched with a residual dipole field. This allows to approximately account for effects of the infinite region around the sphere (even if the so-called infinite element techniques would be more precise). Most of the border of the beam simulation region is at ground potential, so that $\mathbf{E}$ needs to be computed only inside; due to the 3D geometry, $\mathbf{E}$ was computed only in a part (with the domain index $d = 2$), assuming $\mathbf{E} \cong 0$ elsewhere.

Several integration methods are useful, namely: the symplectic partitioned (SP) Runge Kutta (known up to the 8th order)[6]; the leap-frog, with the Boris ordering of electric and magnetic forces (SP2B) [7]; the non symplectic Runge Kutta RK45 (4th and 5th order); here we mainly use a 4th order SP Runge Kutta, but we add a Boris ordering of electric and magnetic forces (SP4B). It is important to define first an uniform framwork, that allows to switch tracing methods and integration steps $\delta s$, especially when crossing domain borders (or passing near electrodes). Let us use $s = ct$ instead of time $t$ and let $o_m$ be the number of

length units in one meter (the geometry is drawn in cm); non-relativistic motion equations are simply

$$\frac{d\mathbf{x}}{ds} = \beta \quad , \quad \frac{d\beta}{ds} = q_1(\mathbf{E} + q_2\beta \times \mathbf{B}) \qquad (1)$$

where $q_1 = q/(mc^2)$, $q_2 = c/o_m$ and $q = -e$ is the electron charge. With the notation $y \equiv (\mathbf{x}, \beta)$ this system is written as $dy/ds = F(y, s)$, which integrated to

$$\frac{y_{n+1} - y_n}{\Delta s} = f(y_n, \Delta s), \quad f = \frac{1}{\Delta s}\int_{s_n}^{s_n + \Delta s} ds\, F(y(s), s) \quad (2)$$

The integration method should return $f$ (by computing $F$ at some points $y$ near $y_n$) and also $d = D(y_n, \Delta s)$ where $d$ is the domain to which these points $y$ belong. If $d$ or $f(y_n, \Delta s)$ significantly change respect to the $n - 1$ step, then $y_{n+1}$ is rejected and $\Delta s$ is decreased until an assigned minimum. This rules avoids large errors at domain borders and near electrodes.

In any integration step, let $y_0 \equiv y^n$ the initial point and $y_M \equiv y^{n+1}$ the final point; for a symplectic integrator $x$ and velocities $\beta$ are separately advanced

$$x_k = x_{k-1} + c_k\Delta s\,\beta_{k-1} \qquad (3)$$

$$\beta_k = \beta_{k-1} + K(x_k, \beta_{k-1}, d_k\Delta s) \qquad (4)$$

for $k = 1, \ldots, M$, where $c_k$ and $d_k$ are tabled weights and $K$ is the kick, that is the velocity increment associated to the $x_k$ point, proportional to the $d_k\Delta s$ length; usually $d_M = 0$, so that only $M - 1$ computations of $K$ are necessary. Without magnetic field $K = q_1\mathbf{E}(x_k)d_k\Delta s$ and the symplectic property is evident, since we have a chain of symplectic transforms. The second order accuracy requires $c_1 = c_2 = \frac{1}{2}$ and $d_1 = 1$, which is the usual leap frog. The choice for the 4th order accuracy is[6, 8, 9]

$$c_1 = c_4 = 1/(4 - 2^{4/3}), \qquad c_2 = c_3 = \frac{1}{2} - c_1 \quad (5)$$

and $d_1 = d_3 = 2c_1$ and $d_2 = 1 - 4c_1$.

Since a magnetic field is present, $K = \beta_k - \beta_{k-1}$ is computed from the sequence[7]

$$\begin{aligned}
\beta^- &= \beta_{k-1} + s_d q_1\mathbf{E}(x_k) \\
\beta^+ &= R[2q_1q_2s_d|B(x_k)|, \hat{\mathbf{B}}]\beta^- \\
\beta_k &= \beta^+ + s_d q_1\mathbf{E}(x_k)
\end{aligned} \qquad (6)$$

where $s_d = d_k\Delta s/2$ and $R(\alpha, \mathbf{n})$ is the rotation by an angle $\alpha$ around the axis $\mathbf{n}$.

An example of beam tracking simulation is given in fig 2. Methods RK45, SP4B and SP2B gave comparable results in first tests with $\Delta s \cong 1$ cm (0.1 cm minimum): the relative error in final energy was within $10^{-3}$. This may be due to the domain changes and to residual errors in the electric field calculation, which is interpolated from finite element solution, without particular refinements (possible, but slower). The work to benchmark methods with an analytic expression (a fit of the computed $\mathbf{E}$) is in an advanced status. In general, noise filtering (independent from solution mesh and based on Poisson eq. properties) should be

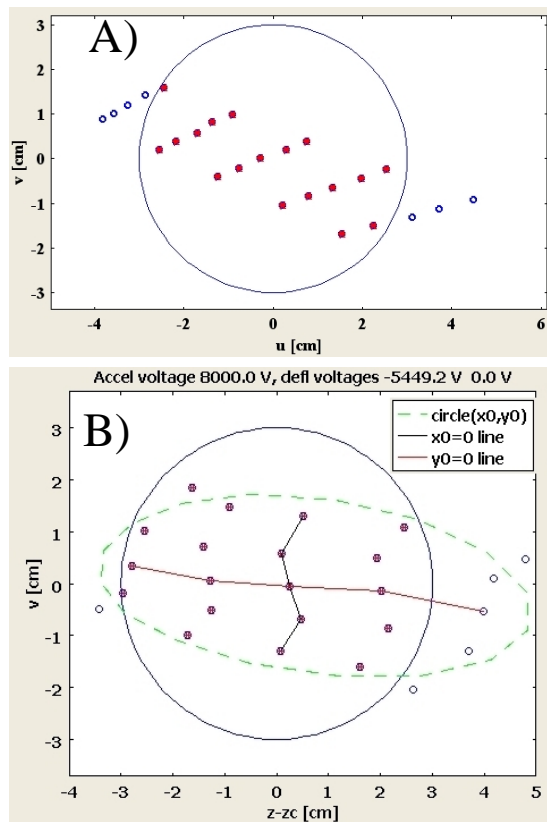Figure 4: Bunch FWHM $t_r$ at collector vs beam energy $E_b$

Figure 3: Beam images of a 0.1 mm spacing $xy$ lattice and a 2.5 mm radius circle, for two starting positions: A) $z = 0.74$ m ; B) $z = -1.4$ m

possible and is considered. Since in our implementation only SP4B and SP2B can work with many particles at a time, they run faster than RK45 (for a set of 41 particles, 350 s and 100 s against 1200 s of CPU on standard 3GHz P4 computer; one core used).

Fig 2 shows a substantial beam oscillation, which may need some corrections with the source inbuilt solenoid and some consideration of self fields. The beam radius is within 2.5 mm at the source and, on the average, it is somewhat compressed by the main solenoid; the deflector optics is strongly magnifying and stigmatic. With the viewport plane coordinates $(u, v)$, where $u = z - z_c$, fig 3B shows an impact map on the lateral viewport; simulation results are roughly independent from the integration method used and in agreement with the observed scintillation light.

## ELECTROSTATIC DIAGNOSTICS

Before removing the P43 three layer phosphor screen (diameter 110 mm) from the $z$-axis, this was used also as a charge collector, thanks to Al coating. The screen both produces scintillation light, showing an $xy$ image, recorded and time integrated by CCD camera, and collects a current $I(t)$ equal to the beam current $I_b(t)$, plus small corrections due to image charges.
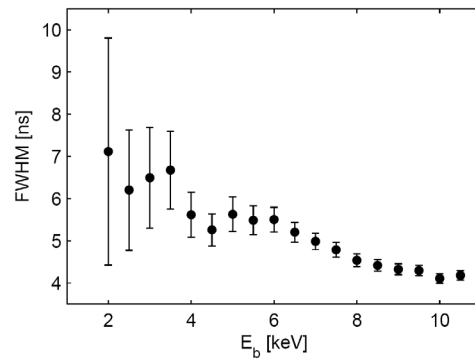
The measuring technique is based on the analytic computation of the voltage $V(t)$ at a DSO (Digital Sampling Oscilloscope), as a function the parameters of $I(t)$ (total charge $Q$, FWHM duration $t_r$), by using standard circuit analysis. We have a large capacitance C (the phosphor screen) connected by a small inductance L (about 5 nH) to a coaxial line terminated at the scope. By fitting $V(t)$ to the actually measured signal $V_M(t)$, the parameter $t_r$ can be measured.

From a plot of $t_r$ against the beam energy $E_b = -eV_s$ we see a small and regular decrease for $E_b > 5$ keV, down to a limit value $t_r = t_m \cong 4$ ns; this can be interpreted as the FWHM pulse duration at source. The bunch lengthening due space charge should go as $E_b^{-3/2}$ and is 2 ns at $E_b = 5$ keV. Below this energy, data are much less regular and may be interpreted as an indication of non adequate beam transport at extraction: the bunch charge increases with $E_b$ when $E_b < 5$ keV, so hindering a trend of FWHM decrease. This interpretation is qualitatively supported by a 1D fluid model.

In conclusion, the Penning-Malmberg machine, designed to study long term evolution of stored electron clouds, can also be efficiently used for time-resolved diagnostics of bunched electron beams.

## REFERENCES

[1] M. Amoretti et al., Rev. Sci. Instrum. **74** (2003) 3991.

[2] B. Paroli et al., *J. Phys. D: Appl. Phys.* **42**, 175203 (5pp) (2009)

[3] M. Cavenago, Nucl. Instrum. Methods, **A 311**, 19 (1992)

[4] D. W. Feldman et al., Proceeding of the 2001 PAC (IEEE, Piscataway, 2001), 2132

[5] http://www.comsol.eu (2007)

[6] H. Yoshida, *Phys. Lett. A*, **150**, 262 (1990).

[7] C. K. Birdsall, A. B. Langdon, *Plasma physics via computer simulation*, Adam Hilger and IOP, Bristol, 1991, p 58-63

[8] M. Suzuki, *Phys. Lett. A*, **146**, 319 (1990)

[9] M. J. Shirakata, H. Fujimori and Y. Irie, p 2655 in EPAC2004, Contribution to the Proceedings, Lucerne, 2004.

**03 Linear Colliders, Lepton Accelerators and New Acceleration Techniques**

**D04 High Intensity in Linear Accelerators - Incoherent Instabilities, Space Char**